Dense Assembly of Gd$_2$O$_3$:0.05X^{3+} (X = Eu, Tb) Nanorods into Nanoscaled Thin-Films and Their Photoluminescence Properties

Jing Huan, Linfeng Hu,* and Xiaosheng Fang*

Department of Materials Science, Fudan University, Shanghai 200433, P. R. China

ABSTRACT: This paper presents a simple and effective oil−water interfacial self-assembly strategy to fabricate monolayer and bilayer nanofilms of densely packed Gd$_2$O$_3$:0.05X^{3+} (X = Eu, Tb) nanorods with characteristic luminescence properties. In this process, Gd$_2$O$_3$:0.05X^{3+} (X = Eu, Tb) nanotubes synthesized by a hydrothermal method are dispersed in deionized water; then, a certain amount of n-hexane is added to produce a hexane−water interface. With n-butanol added as initiator, the nanotubes are gradually trapped at the interface to form a densely packed nanofilm. A monolayer nanofilm of densely packed Gd$_2$O$_3$:0.05Eu^{3+} nanorods is obtained after annealing. In addition, the bilayer nanofilm composed of Gd$_2$O$_3$:0.05X^{3+} (X = Eu, Tb) nanorods still retains the luminescence properties of each monolayer nanofilm. Moreover, the adhesion of the film on the substrate is very strong, which is extremely beneficial for its future applications.

KEYWORDS: interfacial self-assembly, gadolinium oxide, gadolinium hydroxide, bilayer nanofilm, photoluminescence properties
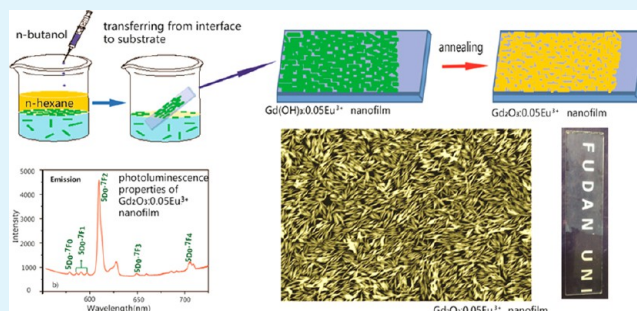
■ INTRODUCTION

Recent years have witnessed the rapid development of electronic and Internet technology, which greatly promoted the upgrading of display technology. Various types of display devices, including liquid crystal display, plasma display, electroluminescent film, the light emitting diode, etc., quickly completed the entire process from the laboratory to factory.[1,2] The manufacture of luminous film, which can achieve the function of mutual conversion of the electrical and optical signals, has always been the core technology of display devices. A variety of chemical and physical strategies has been developed for film preparation, such as electron beam evaporation, magnetron sputtering, molecular beam epitaxy, chemical vapor deposition, Langmuir-Blodgett (LB), and so on.[3−7] Nevertheless, these approaches still have some limitations. For instance, the building blocks for the LB technique usually have to be capped with hydrophobic molecules that keep the nanoparticles stable in the water/air interface.[8] In addition, these techniques usually demand sophisticated equipment and precise control of the process parameters, greatly increasing the manufacturing cost of the film. Consequently, it is essential to develop novel and desirable methods for film preparation.

Most recently, a facile and effective method named "oil−water interface self-assembly" has been reported as a novel chemical approach for film preparation. Pioneering work done by Lin et al. in 2003 found that the liquid−liquid interface can be used as an ideal template for the assembly of nanomaterials.[9] Subsequently, Vanmaekelbergh and Wang et al. researched in detail the physical mechanism of self-assembly at the interface, discovering that the nanostructures can be organized at an oil−water interface to form a high-quality monolayer film due to the decrease of interfacial energy.[10−13] Furthermore, Park et al. reported that it enhanced the densification of the film to add n-dodecanethiol as surfactant into the aqueous phase.[14,15] Sun et al. studied the influence of the initiator amount on film quality.[16] Gagnon et al.[17] studied the effects on the self-assembly of n-alkane/gold nanoparticle mixtures spread at the air−water interface and improved the nanoparticle mobility in the films. Therefore, oil−water interface self-assembly has been frequently used as a simple and universal strategy for the assembly of nanostructures. For example, Duan et al.[18] demonstrated the formation of colloidosomes with shells predominantly composed of monolayers of liquid-like, close-packed nanoparticles based on the interfacial self-assembly of magnetite nanoparticles. Emrick et al.[19] created freestanding nanoparticle monolayers by crosslinking the capping ligands of CdSe nanoparticles self-assembling at water/oil interfaces. Zhong et al.[20] reported the synthesis of hierarchically structured nanocrystals through an interfacial self-assembly driven micro-emulsion (μ-emulsion) process. Since interfacial self-assembly is applicable to a variety of nanostructures including nano-particles and nanotubes, with no need of sophisticated equipment, it has been considered as a low-cost and universal approach of thin-film preparation.

Rare-earth elements have attracted considerable attention because of its unique luminous and magnetic properties. We firstly applied interfacial self-assembly to the preparation of

luminous nanofilm. Toluene was replaced by *n*-hexane with lower toxicity as the oil phase, and dropping rate of the initiator was meticulously adjusted. Well-defined $Eu_{0.05}Gd_{0.95}(OH)_{2.5}Cl_{0.5} \cdot 0.9H_2O$ platelet crystallites were self-assembled at an oil−water interface to form a high-quality nanofilm, which was subsequently annealed to form an oxide nanofilm.[21,22] The as-prepared film exhibited characteristics of Eu^{3+} luminescence properties, leading to good prospects for commercial applications, such as optical/display devices and luminescence probes. In addition, lanthanide-doped inorganic NPs have also received particular interest in biological and biomedical studies. Ren and Qu et al. explored the application of lanthanide-doped nanostructure for targeted imaging and drug delivery.[23−25]

However, two-dimensional (2D) nanostructures, such as nanoplatelets, usually are not considered as the most ideal building blocks of interfacial self-assembly. As the in-plane orientation of the platelet crystallites on the substrate can not be easily controlled, point contact existed between most of the adjacent platelet crystallites, resulting in lots of interspaces. It was difficult for such nanofilms to achieve the highest packing density. The best building blocks for interfacial self-assembly should be one-dimensional (1D) nanostructures including nanowires, nanorods, and nanotubes. When assembled, a large number of 1D nanostructures lay on a substrate; line contact was well formed between adjacent 1D nanostructures, achieving the most compact arrangement. Therefore, if 1D nanostructures of rare-earth oxide materials were assembled into a nanofilm, it would certainly exhibit very high coverage area ratio. Hegmann et al.[26] explored an exceptionally effective and versatile method for the reconfigurable self-assembly of gold nanorods, and Guerrero-Martínez et al.[27] self-assembled core−shell gold−silver nanorods mediated by gemini surfactants for highly efficient SERS-active supercrystals.

It is generally accepted that the morphology of rare-earth hydroxide compounds is quite dependent on the synthetic conditions during the wet-chemical process. The morphology of Er(OH)$_3$ changes from nanosheets to nanotubes as the pH value changes from 7 to 13.[28] High alkaline concentration generally produces 1D rare-earth nanostructures, while 2D $Eu_{0.05}Gd_{0.95}(OH)_{2.5}Cl_{0.5} \cdot 0.9H_2O$ platelet crystallites are prepared in a moderate alkaline condition.[29] Recently, large numbers of outstanding achievements have been made in the synthesis of 1D rare-earth nanostructures. Yang and Lin et al. synthesized one-dimensional La(OH)$_3$:Ln^{3+} (Ln = Yb/Er, Yb/Tm, Yb/Ho) microrods using molten composite-hydroxide (NaOH/KOH) as a solvent[30] and studied the morphologies and structures of Y(OH)$_3$ through a facile and mass production precipitation process using sodium citrate as the shape-control agent.[31] Monodispersed Eu$_2$O$_3$ and Eu$_2$O$_2$S platelet crystallites were obtained by rare-earth organic compounds thermal decomposition in oleic acid/oleylamine and oleic acid/oleylamine/octadecene mixed solution, respectively.[32,33] Li and Xu et al. synthesized rare-earth hydroxide nanotubes with diameter of 20−120 nm by a hydrothermal method.[28,34,35] Yada and Zhang et al. obtained highly crystalline rare-earth oxide nanotubes, with surfactant and polymer as template, respectively.[36,37] However, to the best of our knowledge, there is nearly no report on using 1D rare-earth nanostructures as building blocks by interfacial self-assembly. In this paper, well-defined Gd(OH)$_3$ nanotubes doped with 5% Eu^{3+} (molar ratio) were synthesized via the hydrothermal method. Morphology of the product was precisely controlled by

adjusting temperature, concentration, and pH value of the reaction. Then, these doped hydroxide nanotubes were self-assembled at a hexane−water interface to form a dense and uniform nanofilm, which was subsequently annealed to doped oxide nanofilm with characteristic photoluminescence properties. The transparent nanofilm can emit red light under ultraviolet irradiation, due to the $^5D_0$-^7F_J (J = 0, 1, 2, 3, 4) transitions of Eu^{3+}. Besides, the adhesion of the film on the substrate is so strong that neither immersion in water nor a scratch can make the film peel off from the substrate, which is extremely beneficial for its future applications. The hydrothermal method and interfacial self-assembly were both accessible, and neither of them requires sophisticated equipment. Moreover, the process is applicable to fabricate bilayer nanofilms composed of different rare-earth ions to show tunable photoluminescence properties. Bilayer nanofilms composed of Gd$_2$O$_3$:0.05Eu^{3+} and Gd$_2$O$_3$:0.05Tb^{3+} nanorods have also been successfully fabricated using this method. These results suggest a general way to fabricate oriented films of 1D nanostructures with micrometer size and a transformation way to the production of high-quality rare-earth oxide films. The nanofilms combine many advantages, including characteristic photoluminescence properties, semi-transparency, and strong adhesion on the substrate. Such high-quality films can be applied in sensing devices and various optical/display devices, such as the luminescence panels in field emission displays (FED), plasma display panels (PDP), and so on. As for the optical/display devices, the nanofilm was self-assembled with nanorods, achieving the most compact arrangement, and we can fabricate bilayer nanofilms composed of different rare-earth ions to show tunable photoluminescence properties due to the strong adhesion on the substrate. Furthermore, if the rare-earth nanorods are replaced by some metal nanostructures (e.g., Ag or Au nanoparticles), such self-assembled films can be used as the substrate for surface-enhanced Raman scatting (SERS).[38−40]

■ EXPERIMENTAL SECTION

Materials. Gadolinium chloride hexahydrate (GdCl$_3 \cdot$6H$_2$O, 99.99%), europium chloride hexahydrate (EuCl$_3 \cdot$6H$_2$O, 99.99%), and terbium chloride hexahydrate (TbCl$_3 \cdot$6H$_2$O, 99.99%) were purchased from Alfa Aesar China (Tianjin) Co., Ltd. Sodium hydroxide (NaOH), *n*-hexane, and *n*-butanol were purchased from Sinopharm Chemical Reagent Co., Ltd. (China). Deionized water (≈17 MΩcm$^{−1}$) was used throughout the experiment.

Preparation of Gd(OH)$_3$ Nanotubes. Typically, 400 mg of GdCl$_3 \cdot$6H$_2$O was dissolved in 50 mL of deionized water, along with 21 mg of EuCl$_3 \cdot$6H$_2$O. The pH was adjusted to a pre-set value, generally 11, by using 10% NaOH solution. A white precipitate appeared immediately. After stirring for 10 minutes, the suspension was transferred to a 100 mL autoclave. The autoclave was heated at 140 °C for 12 h. After completion of the reaction, the system was cooled to room temperature. The product of Gd(OH)$_3$:0.05Eu^{3+} nanotubes was filtered and washed by deionized water for several times and then dried at 70 °C. The final powder product was collected for subsequent processing.

Self-Assembly of Gd(OH)$_3$:0.05Eu^{3+} Nanotubes and Thermal Transformation to Gd$_2$O$_3$:0.05Eu^{3+} Nanofilm. Typically, 10 mg of the as-prepared Gd(OH)$_3$:0.05Eu^{3+} nanotube powder was dispersed in 50 mL of deionized water by magnetic stirring for 5 min, and 10 mL of *n*-hexane was added to the vessel to produce a hexane−water interface. Then, 1.5 mL of *n*-butanol was added as initiator to the interface slowly by a syringe, with a typical dropping rate of 0.1 mL/min. The nanotubes were gradually trapped at the interface to form a densely packed nanofilm. Then, most of the *n*-hexane at the top was removed carefully by a syringe, and the film at the interface was transferred to a

Scheme 1. Schematic Illustration of the Fabrication of Gd(OH)₃:0.05X³⁺ Monolayer and Bilayer Nanofilms by Self-Assembly at the Hexane−Water Interface and Annealing Process to Gd₂O₃:0.05X³⁺ Nanofilm
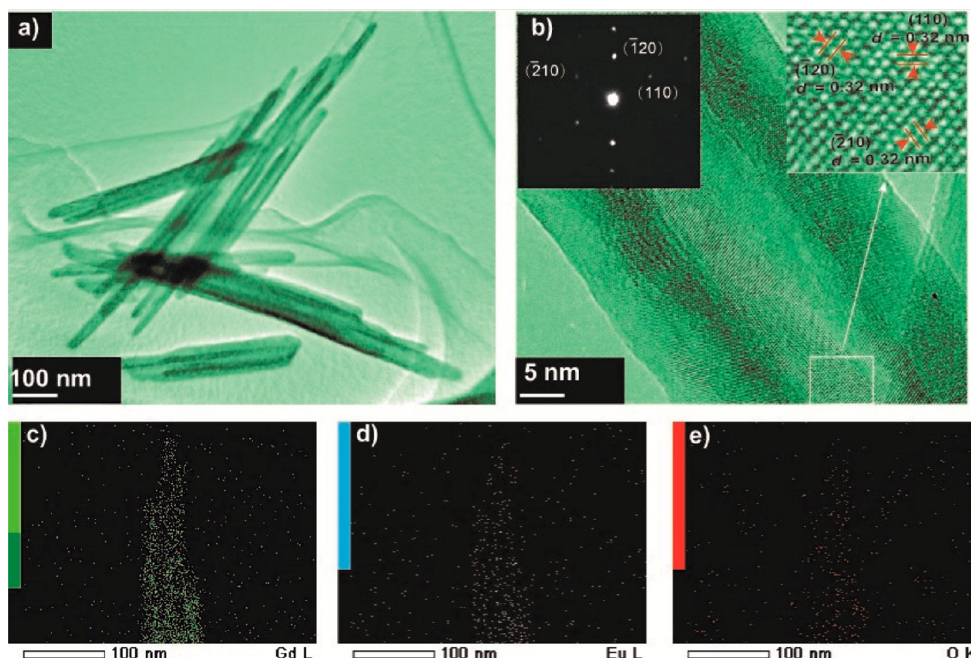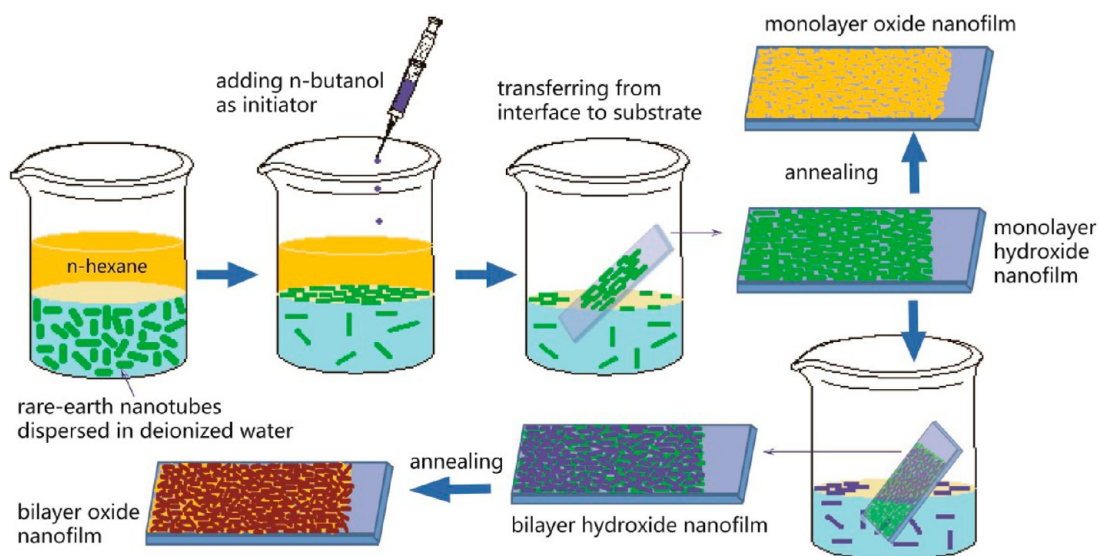
Figure 1. (a) TEM image of Gd(OH)₃:0.05Eu³⁺ nanotubes. (b) HRTEM image of an individual Gd(OH)₃:0.05Eu³⁺ nanotube. The inset shows the SAED pattern taken from an individual Gd(OH)₃:0.05Eu³⁺ nanotube. EDS mapping images of (c) Gd, (d) Eu, and (e) O elements.

quartz substrate by immersing the substrate into the water and pulling it up slowly and carefully. To obtain a bilayer nanofilm, the as-assembled film was dried at room temperature and subsequently repeated the pulling process. Both the monolayer and bilayer nanofilm were annealed at 500 °C for 10 min to oxide nanofilm, as illustrated in Scheme 1.

Characterization. The phase purity and evolution were examined by powder X-ray diffraction (XRD) using a Rigaku RINT-2000 diffractometer with Cu Kα radiation. Scanning electron microscopy (SEM) images were taken with a Keyence VE8800 microscope at an accelerating voltage of 10 kV. Transmission electron microscopy (TEM) images and selected area electron diffraction (SAED) patterns were obtained on a JEOL JEM-3100F energy-filtering (Omega type) transmission microscope. The photoluminescence excitation and emission spectra were measured on a Hitachi F-7000 fluorescence spectrophotometer at room temperature using 700 and 400 V for rare-

earth oxide nanofilm. Thermogravimetry-differential thermal analysis (TG-DTA) measurements were carried out using a Rigaku TGA-8120 instrument in a temperature range of 25−800 °C at a heating rate of 5 °C min⁻¹ under air flow. The nanofilms were analyzed by an atomic force microscope (AFM, SHIMADZ, SPM-9500J3).

■ RESULTS AND DISCUSSION

Preparation of Gd(OH)₃:0.05Eu³⁺ Nanotubes and Its Transformation into Gd₂O₃:Eu³⁺ Nanorods. Gd-(OH)₃:0.05Eu³⁺ nanotubes were synthesized by a facile hydrothermal method as described in the Experimental Section. The temperature and pH value of hydrothermal reaction determines the morphology of the product, including nano-wires, nanorods, nanotubes, or nanosheets. Nanotubes can be
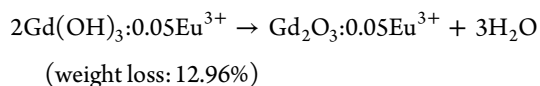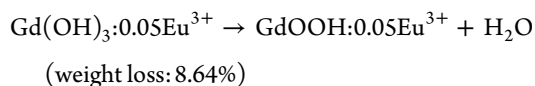
obtained when the pH was adjusted 11 and the autoclave was heated at 140 °C for 12 h. The transmission electron microscopy (TEM) image in Figure 1a shows that the as-obtained nanotubes have an average size of approximately 500 nm in length and 70 nm in diameter. As can be seen from Figure 1b, a high-resolution TEM (HRTEM) image presents clear lattice fringes on an individual nanotube, indicating that the nanotubes are highly crystallized. The inset of Figure 1b shows that the separation between the adjacent fringes is about 3.2 Å, corresponding to the (110), ($\bar{1}$20), and ($\bar{2}$10) plane of the hexagonal $Gd(OH)_3$ crystal. The selected area electron diffraction (SAED) pattern in inset of Figure 1b, taken from an individual nanotube, shows hexagonally arranged sharp diffraction spots, which can be indexed to the [001] zone axis pattern. Figure 1c–e shows the energy dispersive X-ray spectroscopy (EDS) mapping of Gd, Eu, and O elements, respectively, in the $Gd(OH)_3$:0.05Eu^{3+} nanotubes. As can be seen, Gd, Eu, and O elements are uniformly distributed in the crystal and the mapping intensity is proportional to the content of every element. These results indicate that the Eu element may be successfully doped into $Gd(OH)_3$ crystal to form uniform solid solution samples.

Thermogravimetric (TGA) analysis was carried out to explore the phase conversion of the as-prepared $Gd(OH)_3$:0.05Eu^{3+} nanotubes through a heat treatment process. The thermogravimetric curve is shown in Figure 2; the
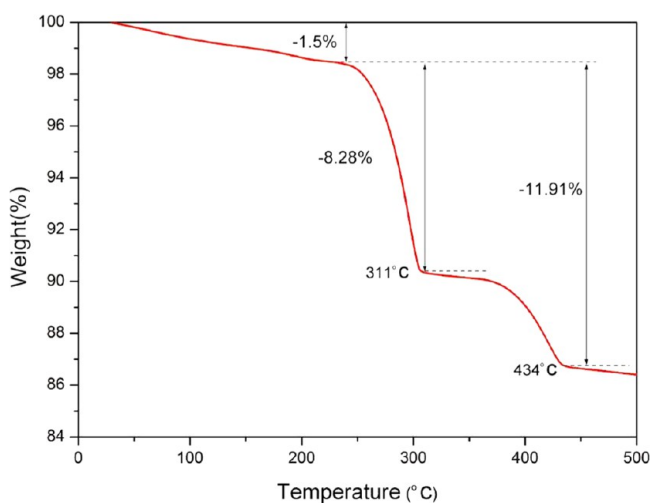
Figure 2. TGA curves of the as-prepared $Gd(OH)_3$:0.05Eu^{3+} nanotube powder (heating rate: 5 °C/min).

approximate 1.5% weight loss below 200 °C can be attributed to the evaporation of adsorbed water on the surface of nanotubes. The 8.28 % and 11.91 % weight loss at 311 and 434 °C can be considered as the mass loss of the transfer from $Gd(OH)_3$:0.05Eu^{3+} to $GdOOH$:0.05Eu^{3+} and Gd_2O_3:0.05Eu^{3+}, respectively. This is almost consistent with the calculation results, 8.64 % and 12.96 %, respectively. The reaction could be expressed by the following equation:

$$Gd(OH)_3{:}0.05Eu^{3+} \rightarrow GdOOH{:}0.05Eu^{3+} + H_2O$$

(weight loss: 8.64%)

$$2Gd(OH)_3{:}0.05Eu^{3+} \rightarrow Gd_2O_3{:}0.05Eu^{3+} + 3H_2O$$

(weight loss: 12.96%)

From the TGA analysis, one can see that the annealing temperature of more than 450 °C is high enough to complete the phase conversion from the rare-earth hydroxides to the oxides. Generally, the photoluminescence intensity of rare-earth hydroxides is much lower than the rare-earth oxides due to the existence of nonradiative relaxation channels provided by high-energy vibration of hydroxyl species.[41] Therefore, compared with rare-earth hydroxide precursor, rare-earth oxides often exhibit superior photoluminescence properties and have more potentialities for practical applications. Besides, the hydroxides can serve as an ideal precursor template for the corresponding oxides. These reasons inspire us to consider the thermal transformation from a rare-earth hydroxide film into the corresponding oxide film.

The as-prepared $Gd(OH)_3$:0.05Eu^{3+} nanotubes were subsequently heated slowly up to 500 °C and maintained for 10 min. As shown in Figure 3a, the framework of the nanotubes was well maintained after the annealing process. The crystallinity was improved, which can be proved subsequently by the much higher intensity of diffraction peaks in Figure 5. However, the tubular shape collapsed during the heat treatment procedure, and most of the products after annealing exhibit nanorod morphology. Figure 3b shows that the crystal system has changed from hexagonal phase to cubic phase, confirming the conversion from $Gd(OH)_3$:0.05Eu^{3+} to Gd_2O_3:0.05Eu^{3+}. The separation between the adjacent fringes is 5.4 Å, corresponding to the (200) and (020) plane of the body-centered Gd_2O_3 crystal. The SAED pattern in the inset of Figure 3b, taken from an individual nanorod, shows cubically arranged sharp diffraction spots, which can be indexed to the [001] zone axis pattern. Meanwhile, the uniform distribution of Gd, Eu, and O elements in the crystal remains, as shown in Figure 3c–e.

Self-Assembly of $Gd(OH)_3$:0.05Eu^{3+} Nanotubes into High-Quality Nanofilms and Thermal Transformation. A high-quality nanofilm of $Gd(OH)_3$:0.05Eu^{3+} nanotubes was prepared by self-assembly strategy at an oil−water interface, which is detailed in the Experimental Section. Similar to a previous study,[20] an appropriate quantity of *n*-butanol is crucial for the formation of film with a desirable quality. Too little *n*-butanol results in a low area coverage ratio, whereas too much *n*-butanol leads to the obvious overlapping of nanotubes. Furthermore, the residual *n*-hexane adversely affects the adhesion of the film on the substrate, making the transfer of the film from the interface to the substrate more difficult. Therefore, after removing most of the *n*-hexane at the top by a syringe, the system was kept in a fume hood for sometime so that the remaining *n*-hexane could completely evaporate. Then, the transfer from the air−water interface to the substrate became much easier.

According to previous studies on oil−water interfacial self-assembly strategies, the decrease in the interfacial energy was considered as the driving force of self-assembly.[10−13,42−44] We have studied the mechanism of the oil−water interfacial self-assembly of nanoparticles in detail in our previous work,[8] which can be easily applied to the oil−water interfacial self-assembly of nanorods in this manuscript. *n*-Butanol was regarded as the inducer of the self-assembly, which was adsorbed on the surfaces of the nanorods, decreasing the surface charge of the nanorods and rendering those around the interface very active. The nanorods were assembled at the interface after they gained enough activity, driven by the minimization of interfacial
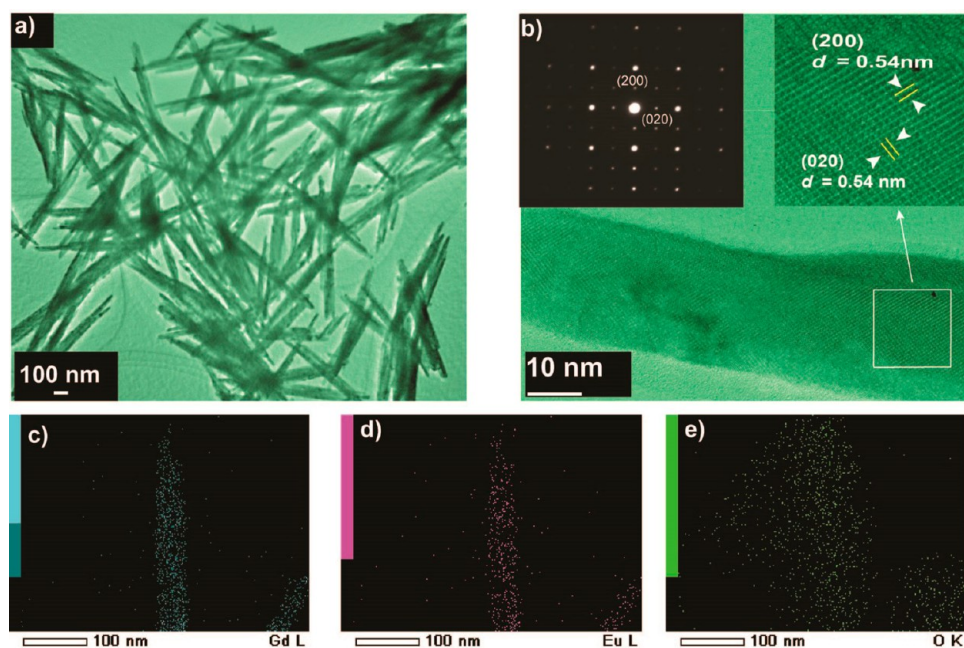
Figure 3. (a) TEM image of Gd_2O_3:0.05Eu^{3+} nanorods. (b) HRTEM image of an individual Gd_2O_3:0.05Eu^{3+} nanorod. The inset shows the SAED pattern taken from an individual Gd_2O_3:0.05Eu^{3+} nanorod. EDS mapping images of (c) Gd, (d) Eu, and (e) O elements.

energy. As a result, the nanorods prefer to be trapped in the oil−water interface to form a closely packed nanofilm.

The $Gd(OH)_3$:0.05Eu^{3+} nanofilm precursor was heated to obtain Gd_2O_3:0.05Eu^{3+} nanofilm. The annealing process was carried out at 500 °C for 10 min. Figure 4a,b displays the
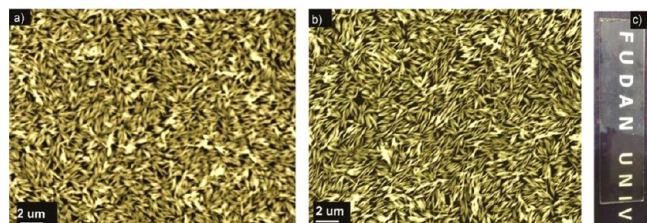

Figure 4. Top-view SEM images of the nanofilms (a) before and (b) after annealing. (c) The photograph of the transparent nanofilm after annealing.

scanning electron microscopy (SEM) image of the nanofilms before and after annealing, respectively. As can be seen from the $Gd(OH)_3$:0.05Eu^{3+} nanofilm, the substrate is densely covered with a large number of 1D nanotubes. The nanotubes are neatly tiled with their edges in contact basically side-by-side. The area coverage ratio is apparently improved compared with the nanofilm self-assembled from 2D nanoplatelets in our previous work, justifying the effective utilization of the 1D nanostructures as the building blocks.[21] The annealing process accomplished the conversation from $Gd(OH)_3$:0.05Eu^{3+} to Gd_2O_3:0.05Eu^{3+}, while the well-defined morphology, densification, and uniformity were well maintained. As shown in Figure 4c, the nanofilm was highly continuous and uniform at the macroscopic scale, and it was quite transparent to visible light. Besides, the nanorods in the oxide film were more tightly adhered to the substrate compared to those in the precursor film. Neither immersion in water nor a scratch could make the film peel off from the substrate. This demonstrates that the annealing process enhanced the adhesion of the film on the

substrate, which is extremely beneficial for its future practical applications.

X-ray diffraction (XRD) characterization of the nanofilms before and after the annealing process was carried out to identify the phase transfer. Figure 5 shows the XRD patterns of
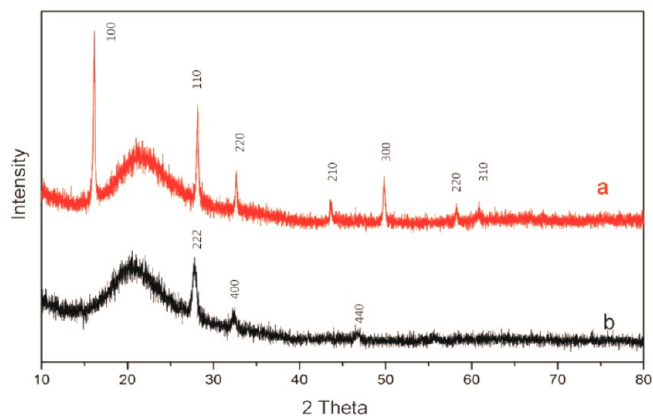

Figure 5. X-ray diffraction patterns of the as-assembled nanofilms (a) before and (b) after annealing.

the film before and after annealing. For the sample before annealing, all diffraction peaks can be indexed to a pure hexagonal $Gd(OH)_3$:0.05Eu^{3+} phase. For the sample after annealing, although the broad peak in the low-range region from 15° to 25° caused by the amorphous glass substrate covered the (211) peak of Gd_2O_3:0.05Eu^{3+}, (222), (400), and (440) diffraction peaks are still detected.

The atomic force microscope (AFM) images of the nanofilm before and after annealing were shown in Figure 6. The as-transformed oxide film shows a smooth surface, and the nanorods on the substrate were extremely compact. There was almost no interspace between adjacent nanorods. In addition, the thickness of the film decreased after annealing, with an average height decreasing from ∼127 to ∼83 nm. This was
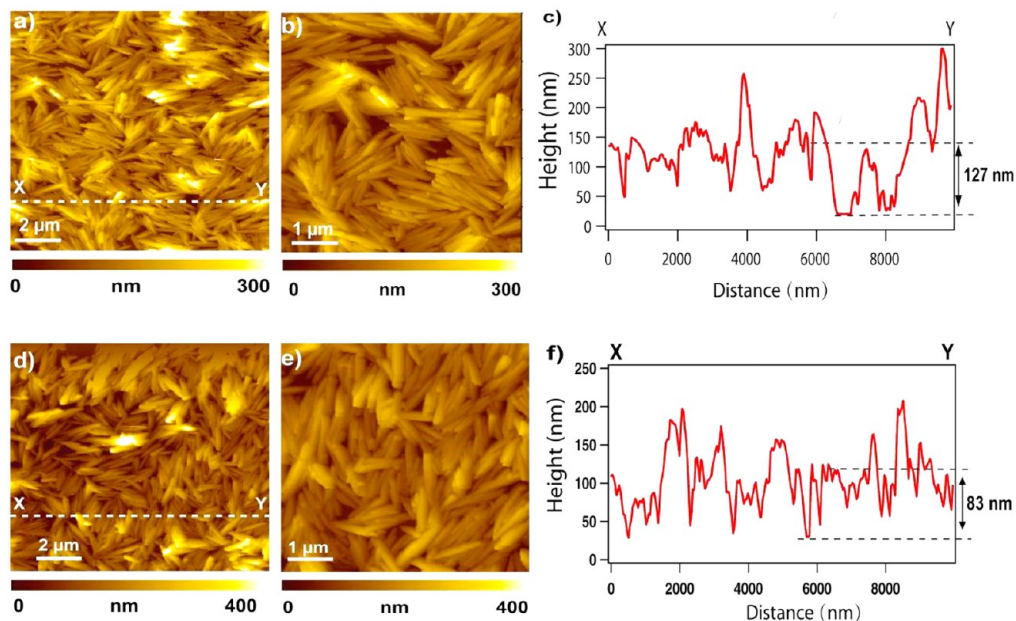
Figure 6. AFM images of the nanofilms (a, b) before and (d, e) after annealing. (c) and (f) are thickness information of the nanofilms before and after annealing, respectively.
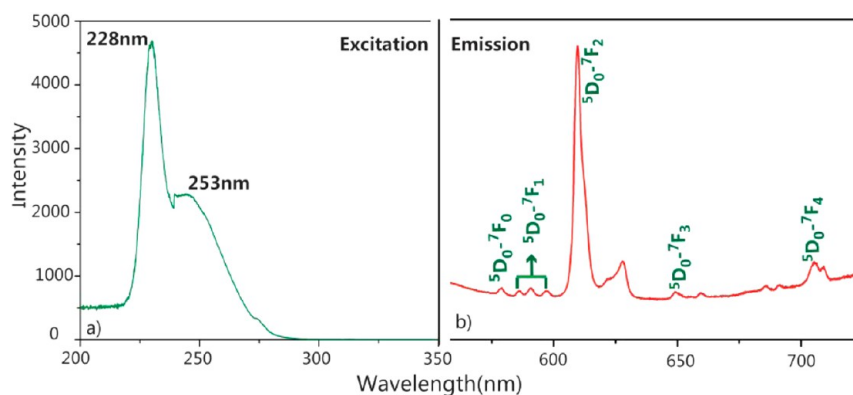
Figure 7. (a) Excitation spectrum of Gd_2O_3:$0.05Eu^{3+}$ nanofilm monitored at 613 nm and (b) emission spectrum of Gd_2O_3:$0.05Eu^{3+}$ nanofilm excited at 228 nm.

mainly caused by lattice contraction of the conversation from hydroxide to oxide.

Photoluminescence Property of the Gd_2O_3:$0.05Eu^{3+}$ Nanofilm. Photoluminescence property of the Gd_2O_3:$0.05Eu^{3+}$ nanofilm was explored by excitation and emission spectra. The excitation spectrum and emission spectrum of the as-transformed film were displayed in Figure 7. A sharp emission peak at 613 nm was observed under ultraviolet irradiation, yielding a red light emission. Excitation spectra monitored at 613 nm was shown in Figure 7a; two excitation peaks appeared at 228 and 253 nm. The emission through the former exhibited a slightly higher intensity than the latter. The excitation peak at 228 nm can be attributed to the Gd_2O_3 host excitation band. When the samples are excited by UV irradiation, the energy is absorbed by the Gd_2O_3 host, inducing the electronic transition from the energy level of valence band to the conduction band of the Gd_2O_3 host. Some of the electrons in the excited levels of conduction band transfer to the $^5D_0$ level of Eu^{3+} and then to the ^5F_J (J = 0, 1, 2, 3, 4) levels of Eu^{3+}, yielding the Eu^{3+} emissions. The excitation peak at 253 nm is ascribed to the Eu^{3+}-O^{2-} charge transfer

(CT) band. The charge transfer transition generally occurs when electrons transfer from the 2p orbital of O^{2-} towards 4f orbital of Eu^{3+}, resulting in the Eu^{3+} emission.[45] Figure 7b shows the emission spectrum excited at 228 nm. The emission peaks at 582, 589−601, 613, 654, and 709 nm were assigned to $^5D_0$-^7F_J (J = 0, 1, 2, 3, 4) transitions of Eu^{3+}, respectively.

Bilayer Nanofilms Composed of Gd_2O_3:$0.05Eu^{3+}$ and Gd_2O_3:$0.05Tb^{3+}$ Nanorods. Due to the similar atomic structure of Eu and Tb, the previous process can be applied to obtain Gd_2O_3:$0.05Tb^{3+}$ nanofilms. More importantly, the bilayer nanofilm was obtained by self-assembling Gd_2O_3:$0.05Eu^{3+}$ and Gd_2O_3:$0.05Tb^{3+}$ nanorods in succession. As can be seen from Figure 8a, the Gd_2O_3:$0.05Eu^{3+}$/ Gd_2O_3:$0.05Tb^{3+}$ bilayer nanofilm was highly continuous and uniform at the macroscopic scale, just like the monolayer nanofilm. Such a bilayer film is still transparent due to its nanoscaled thickness, as shown in Figure 8b.

The main difference between Gd_2O_3:$0.05Eu^{3+}$ and Gd_2O_3:$0.05Tb^{3+}$ is in luminescence properties. Under ultraviolet irradiation, Gd_2O_3:$0.05Eu^{3+}$ emits red light while Gd_2O_3:$0.05Tb^{3+}$ emits green light. When Gd_2O_3:$0.05Eu^{3+}$
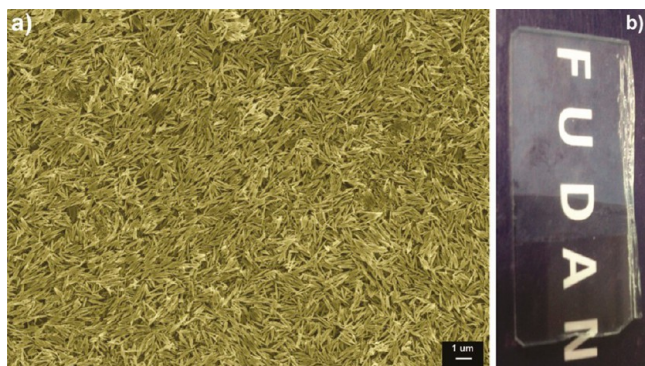
Figure 8. (a) Top-view SEM images of the bilayer nanofilm composed of Gd_2O_3:$0.05Eu^{3+}$ and Gd_2O_3:$0.05Tb^{3+}$ nanorods after annealing and (b) the photograph of the transparent nanofilm.

and Gd_2O_3:$0.05Tb^{3+}$ nanorods were self-assembled in succession to obtain a bilayer nanofilm, the bilayer nanofilm shows luminescence properties composed of typical emission from both Eu^{3+} and Tb^{3+}. The emission spectrum of the bilayer nanofilm is shown in Figure 9. The emission peak of Gd_2O_3:$0.05Tb^{3+}$ appeared at 543 nm, assigned to the $^5D_4$-$^7F_5$ transition of Tb^{3+}. To avoid the typical emission peak of Gd_2O_3:$0.05Tb^{3+}$ being covered by the double frequency peak, the excitation frequency was chosen at 280 nm and the emission spectrum was scanned separately, from 470 to 550 nm (Figure 9a) and from 580 to 720 nm (Figure 9b). Under such excitation conditions, the intensity of the Gd_2O_3:$0.05Eu^{3+}$ emission spectrum was much lower than that excited by 228 and 253 nm. However, the typical emission peak of Gd_2O_3:$0.05Eu^{3+}$ can still be clearly detected, as shown in Figure 9b. Meanwhile, the emission peak of Gd_2O_3:$0.05Tb^{3+}$ was also observed at 485 and 543 nm, assigned to $^5D_4$-$^7F_6$ and $^5D_4$-$^7F_5$ transitions of Tb^{3+}, respectively, as shown in Figure 9a. The bilayer nanofilm exhibits both the luminescence properties of Gd_2O_3:$0.05Eu^{3+}$ and Gd_2O_3:$0.05Tb^{3+}$ emission, which is of great potential for future applications.

CONCLUSIONS

In summary, a simple, effective, and universal strategy to fabricate a nanofilm with characteristic luminescence properties was presented in this work. $Gd(OH)_3$:$0.05Eu^{3+}$ nanotubes were synthesized via the hydrothermal method and then self-assembled at a hexane–water interface to form a monolayer nanofilm. A nanofilm of densely packed Gd_2O_3:$0.05Eu$ nanorods was obtained after annealing. The nanofilm was highly continuous and uniform at the macroscopic scale, and it was more compact compared with nanofilms self-assembled with 2D nanostructures. The nanofilm exhibited characteristic luminescence properties. It was transparent to visible light while emitting red and green light, respectively, under ultraviolet irradiation. Moreover, the bilayer nanofilm composed of Gd_2O_3:$0.05Eu^{3+}$ and Gd_2O_3:$0.05Tb^{3+}$ nanorods maintained the luminescence properties of each monolayer nanofilm. Furthermore, the strong adhesion of the nanofilm on the substrate was extremely beneficial for its future applications.

AUTHOR INFORMATION

Corresponding Authors
*E-mail: linfenghu@fudan.edu.cn. Tel/Fax: (+86) 21-6564-2996 (L. F. Hu).
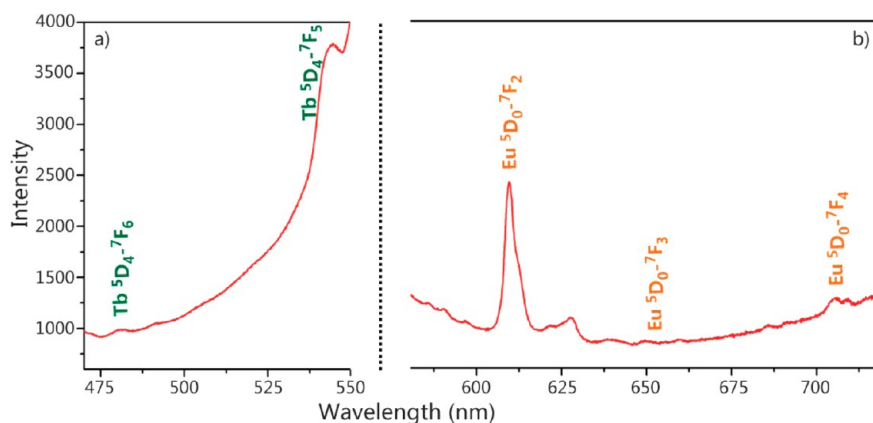*E-mail: xshfang@fudan.edu.cn. Tel/Fax: (+86) 21-6564-2996 (X. S. Fang).

Notes
The authors declare no competing financial interest.

REFERENCES

(1) Kazan, B. *Science* **1980**, *208*, 927−936.
(2) Drzaic, P. *Nat. Photonics* **2009**, *3*, 248−249.
(3) Choe, J. Y.; Ravichandran, D.; Blomquist, S. M.; Morton, D. C.; Kirchner, K. W.; Ervin, M. H.; Lee, U. *Appl. Phys. Lett.* **2001**, *78*, 3800−3802.
(4) Wan, Y.; Zhao, D. Y. *Chem. Rev.* **2007**, *107*, 2821−2860.

Figure 9. The emission spectra of the bilayer nanofilm excited at 280 nm, scanned from (a) 470 to 550 nm and (b) 580 to 720 nm.

(5) Reuter, S.; Hofmann, A. M.; Busse, K.; Frey, H.; Kressler, J. *Langmuir* **2011**, *27*, 1978−1989.

(6) Tao, A. R.; Huang, J.; Yang, P. *Acc. Chem. Res.* **2008**, *41*, 1662−1673.

(7) Li, L.; Zhai, T. Y.; Zeng, H. B.; Fang, X. S.; Bando, Y.; Golberg, D. *J. Mater. Chem.* **2011**, *21*, 40−56.

(8) Ren, Y.; Chen, M.; Hu, L. F.; Fang, X. S.; Wu, L. M. *J. Mater. Chem.* **2012**, *22*, 944−950.

(9) Lin, Y.; Skaff, H.; Emrick, T.; Dinsmore, A. D.; Russell, T. P. *Science* **2003**, *299*, 226−229.

(10) Reincke, F.; Hickey, S. G.; Kegel, W. K.; Vanmaekelbergh, D. *Angew. Chem., Int. Ed.* **2004**, *43*, 458−462.

(11) Wang, J.; Wang, D.; Sobal, N. S.; Giersig, M.; Jiang, M.; Möhwald, H. *Angew. Chem., Int. Ed.* **2006**, *45*, 7963−7966.

(12) Wang, D.; Duan, H.; Mohwald, H. *Soft Matter* **2005**, *1*, 412−416.

(13) Xia, H.; Wang, D. Y. *Adv. Mater.* **2008**, *20*, 4253−4256.

(14) Park, Y.; Yoo, S.; Park, S. *Langmuir* **2007**, *23*, 10505−10510.

(15) Yun, S.; Park, Y.; Kim, S. K.; Park, S. *Anal. Chem.* **2007**, *79*, 8584−8589.

(16) Li, Y.; Huang, W.; Sun, S. *Angew. Chem., Int. Ed.* **2006**, *45*, 2537−2539.

(17) Gagnon, B. P.; Meli, M. V. *Langmuir*, DOI: 10.1021/la4037937 (accessed Dec 20, 2013).

(18) Duan, H.; Wang, D. Y.; Sobal, N. S.; Giersig, M.; Kurth, D. G.; Möhwald, H. *Nano Lett.* **2005**, *5*, 949−952.

(19) Lin, Y.; Skaff, H.; Böker, A.; Dinsmore, A. D.; Emrick, T.; Russell, T. P. *J. Am. Chem. Soc.* **2003**, *125*, 12690−12691.

(20) Zhong, Y.; Wang, Z.; Zhang, R.; Bai, F.; Wu, H.; Haddad, R.; Fan, H. *ACS Nano*, DOI: 10.1021/nn405492d (accessed Dec 18, 2013).

(21) Hu, L. F.; Ma, R. Z.; Ozawa, T. C.; Sasaki, T. *Angew. Chem., Int. Ed.* **2009**, *48*, 3846−3849.

(22) Hu, L. F.; Ma, R. Z.; Ozawa, T. C.; Geng, F. X.; Iyi, N.; Sasaki, T. *Chem. Commun.* **2008**, 4897−4899.

(23) Liu, Z.; Liu, X.; Yuan, Q.; Dong, K.; Jiang, L.; Li, Z.; Ren, J.; Qu, X. *J. Mater. Chem.* **2012**, *22*, 14982−14990.

(24) Zhou, L.; Li, Z.; Ju, E.; Liu, Z.; Ren, J.; Qu, X. *Small* **2013**, *9*, 4262−4268.

(25) Liu, Z.; Ju, E. G.; Liu, J. H.; Du, Y. D.; Li, Z. Q.; Yang, Q. H.; Ren, J. S.; Qu, X. G. *Biomaterials* **2013**, *34*, 7444−7452.

(26) Umadevi, S.; Feng, X.; Hegmann, T. *Adv. Funct. Mater.* **2013**, *23*, 1393−1403.

(27) Gómez-Graña, S.; Pérez-Juste, J.; Alvarez-Puebla, R. A.; Guerrero-Martínez, A.; Liz-Marzán, L. M. *Adv. Opt. Mater.* **2013**, *1*, 477−481.

(28) Wang, X.; Li, Y. D. *Chem.—Eur. J.* **2003**, *9*, 5627−5635.

(29) Geng, F. X.; Matsushita, Y.; Ma, R.; Xin, H.; Tanaka, M.; Izumi, F.; Iyi, N.; Sasaki, T. *J. Am. Chem. Soc.* **2008**, *130*, 16344−16350.

(30) Zhang, X.; Yang, P.; Wang, D.; Xu, J.; Li, C.; Gai, S.; Lin, J. *Cryst. Growth Des.* **2011**, *12*, 306−312.

(31) Huang, S.; Xu, J.; Zhang, Z.; Zhang, X.; Wang, L.; Gai, S.; He, F.; Niu, N.; Zhang, M.; Yang, P. *J. Mater. Chem.* **2012**, *22*, 16136−16144.

(32) Si, R.; Zhang, Y. W.; You, L. P.; Yan, C. H. *Angew. Chem., Int. Ed.* **2005**, *44*, 3256−3260.

(33) Zhao, F.; Yuan, M.; Zhang, W.; Gao, S. *J. Am. Chem. Soc.* **2006**, *128*, 11758−11759.

(34) Wang, X.; Sun, X. M.; Yu, D.; Zou, B. S.; Li, Y. D. *Adv. Mater.* **2003**, *15*, 1442−1445.

(35) Fang, Y. P.; Xu, A. W.; You, L. P.; Song, R. Q.; Yu, J. C.; Zhang, H. X.; Li, Q.; Liu, H. Q. *Adv. Funct. Mater.* **2003**, *13*, 955−960.

(36) Yada, M.; Mihara, M.; Mouri, S.; Kuroki, M.; Kijima, T. *Adv. Mater.* **2002**, *14*, 309−313.

(37) Wu, G. S.; Lin, Y.; Yuan, X. Y.; Xie, T.; Cheng, B. C.; Zhang, L. D. *Nanotechnology* **2004**, *15*, 568−571.

(38) Orendorff, C. J.; Gole, A.; Sau, T. K.; Murphy, C. J. *Anal. Chem. (Washington, DC, U. S.)* **2005**, *77*, 3261−3266.

(39) Liberman, V.; Yilmaz, C.; Bloomstein, T. M.; Somu, S.; Echegoyen, Y.; Busnaina, A.; Cann, S. G.; Krohn, K. E.; Marchant, M. F.; Rothschild, M. *Adv. Mater.* **2010**, *22*, 4298−4302.

(40) Yap, F. L.; Thoniyot, P.; Krishnan, S.; Krishnamoorthy, S. *ACS Nano* **2012**, *6*, 2056−2070.

(41) Matsumoto, Y.; Unal, U.; Kimura, Y.; Ohashi, S.; Izawa, K. *J. Phys. Chem. B* **2005**, *109*, 12748−12754.

(42) Reincke, F.; Kegel, W. K.; Zhang, H.; Nolte, M.; Wang, D.; Vanmaekelbergh, D.; Möhwald, H. *Phys. Chem. Chem. Phys.* **2006**, *8*, 3828−3835.

(43) Kutuzov, S.; He, J.; Tangirala, R.; Emrick, T.; Russell, T. P.; Böker, A. *Phys. Chem. Chem. Phys.* **2007**, *9*, 6351−6358.

(44) Niu, Z.; He, J.; Russell, T. P.; Wang, Q. *Angew. Chem., Int. Ed.* **2010**, *49*, 10052−10066.

(45) Pang, M. L.; Lin, J.; Fu, J.; Xing, R. B.; Luo, C. X.; Han, Y. C. *Opt. Mater.* **2003**, *23*, 547−558.